Journal of Biomechanical Engineering. Received July 14, 2021;
Accepted manuscript posted December 05, 2021. doi:10.1115/1.4053143
Copyright (c) 2021 by ASME; reuse license CC-BY 4.0

Check for updates

Confined cell migration and asymmetric hydraulic environments to evaluate the metastatic potential of cancer cells

Yago Juste-Lanas [1,2,§], Pedro Enrique Guerrero [1,§], Daniel Camacho-Gómez [1], Silvia Hervás-Raluy [1], Jose M García-Aznar [1], María J Gomez-Benito [1] +

Affiliations: [1] Department of Mechanical Engineering, University of Zaragoza, Zaragoza, Spain; [2] Department of Biochemistry and Molecular and Cellular Biology, University of Zaragoza, Zaragoza, Spain

§: Both authors contributed equally to this work.

Correspondence: Department of Mechanical Engineering, University of Zaragoza, Zaragoza, Spain. e-mail: gomezmj@unizar.es

Accepted Manuscript Not Copyedited

Downloaded from http://asmedigitalcollection.asme.org/biomechanical/article-pdf/doi/10.1115/1.4053143/6806175/bio-21-1259.pdf by Universidad De Zaragoza Biblioteca user on 10 January 2022

Abstract

Metastasis, a hallmark of cancer development, is also the leading reason for most cancer-related deaths. Furthermore, cancer cells are highly adaptable to microenvironments and can migrate along pre-existing channel-like tracks of anatomical structures. However, more representative three-dimensional models are required to reproduce the heterogeneity of metastatic cell migration *in vivo* to further understand the metastasis mechanism and develop novel therapeutic strategies against it. Here, we designed and fabricated different microfluidic-based devices that recreate confined migration and diverse environments with asymmetric hydraulic resistances. Our results show different migratory potential between metastatic and nonmetastatic cancer cells in confined environments. Moreover, although nonmetastatic cells have not been tested against barotaxis due to their low migration capacity, metastatic cells present an enhanced preference to migrate through the lowest resistance path, being sensitive to barotaxis. This device, approaching the study of metastasis capability based on confined cell migration and barotactic cell decisions, may pave the way for the implementation of such technology to determine and screen the metastatic potential of certain cancer cells.

Journal of Biomechanical Engineering. Received July 14, 2021;
Accepted manuscript posted December 05, 2021. doi:10.1115/1.4053143
Copyright (c) 2021 by ASME; reuse license CC-BY 4.0

Key terms

Microfluidic device, confined migration, single cell, barotaxis, hydraulic resistance, metastasis

Accepted Manuscript Not Copyedited

Downloaded from http://asmedigitalcollection.asme.org/biomechanical/article-pdf/doi/10.1115/1.4053143/6806175/bio-21-1259.pdf by Universidad De Zaragoza Biblioteca user on 10 January 2022

Journal of Biomechanical Engineering. Received July 14, 2021;
Accepted manuscript posted December 05, 2021. doi:10.1115/1.4053143
Copyright (c) 2021 by ASME; reuse license CC-BY 4.0

Introduction

Invasion and metastasis are the most dangerous hallmarks of cancer development [1], [2], a multistage process where cancer cells spread and colonize distant organs. Unfortunately, despite remarkable progress in the field of cancer research, it still represents one of the leading reasons for most cancer-related deaths [3], [4]. Metastatic cells have acquired the ability to invade the surrounding tissues, leading to the formation of secondary tumors. This journey entails a series of multistep stages. It commonly comprises cell dissociation from the primary tumor and epithelial-to-mesenchymal transition (EMT) [5]. Later, motile cells usually go through different physical barriers, such as the basement membrane and the extracellular matrix (ECM). This drive ends with intravasation to the microvasculature of the lymph and blood systems as one of the last steps before motile cancer cells extravasate and spread to new locations [6], [7].

In vivo, motile cancer cells undergoing metastasis are highly adaptable to the physico-chemical properties of a wide variety of microenvironments. Generally, surrounding tissue invasion involves cell migration along pre-existing channel-like tracks of anatomical structures or by degrading the extracellular matrix if no pathway is available [8]–[10]. Furthermore, mechanosensing feedback and cytoskeletal rearrangement for drastic changes in cell shape are essential for invasive cancer cells in heterogeneous microenvironments, which usually include confined and constricting spaces narrower than the cell diameter [11], [12].

In the last few decades, we have witnessed an extraordinary advance in cancer research as a result of a vast effort in the scientific community, and recently, several molecular markers have been successfully related to the metastatic potential of certain tumors [13]. However, the prediction of the metastatic potential of certain tumors still represents an unsolved challenge. Classical models of cell migration have typically been studied in two dimensions [14], [15]. Nevertheless, those models do not accurately represent the real three-dimensional (3D) microenvironment present under *in vivo* cell migration. Thus, more representative 3D models are required to reproduce the heterogeneity of metastatic cell migration *in vivo* [16], [17]. To overcome this limitation, microfluidic devices are helpful tools [18]. They can be used to recreate

Accepted Manuscript Not Copyedited

Downloaded from http://asmedigitalcollection.asme.org/biomechanical/article-pdf/doi/10.1115/1.4053143/6806175/bio-21-1259.pdf by Universidad De Zaragoza Biblioteca user on 10 January 2022

Journal of Biomechanical Engineering. Received July 14, 2021;
Accepted manuscript posted December 05, 2021. doi:10.1115/1.4053143
Copyright (c) 2021 by ASME; reuse license CC-BY 4.0

different cell migration-inducing mechanisms that rely on biochemical, mechanical and topographical properties of the surrounding environment [19]–[22]. At the same time, a better understanding of the mechanisms by which cells migrate may lead to the development of novel therapeutic strategies for controlling tumor invasiveness and metastasis, mainly known as migrastatic drugs [23].

One of these mechanisms that regulates cell migration is barotaxis [24]. It mainly arises when confined cells move through low-permeability environments [24], [25]. Under these conditions, cells have to displace the surrounding fluid to migrate, thus generating a pressure drop between the front of the cell and the end of its path. This pressure drop is proportional to the column of fluid the cell has to displace, namely, hydraulic resistance [24], [26]. Such resistance is known to play a critical role in cell orientation, polarization and migration itself [27]. Prentice-Mott *et al.* [28], pioneers in this field, revealed that leukocyte-like cells surrounded by asymmetric hydraulic environments are able to identify the path that poses the lowest hydraulic resistance. They observed that in certain cell types, the physical properties of the surrounding environment alone affect the decision-making process of directional cell migration and can even outcompete the impact of chemical properties [28], [29]. Notwithstanding, this mechanism has been poorly studied in cancer cells.

The goal of this work was to develop microfluidic devices with confined migration channels and bifurcating pathways of different hydraulic resistances. These devices aim to shed light on cancer cell migration and barotaxis and thus to help screen metastatic cells and decipher the mechanism beyond the capability of certain tumor cells to undergo metastasis. Specifically, we designed and fabricated (I) devices that recreate confined migration and two paths of asymmetric hydraulic resistance; (II) negative-control devices, with symmetric paths; and (III) positive-control devices, with a dead end in one of their paths. Furthermore, we fabricated (IV) devices with similar hydraulic resistances but different levels of tortuosity, to determine if the capacity of the cell to sense different hydraulic resistances could be biased by the topology of the device.

Therefore, to study cancer cell migration in confined environments and to determine if this migration is influenced by barotaxis, we used two different common cell lines of

Accepted Manuscript Not Copyedited

Downloaded from http://asmedigitalcollection.asme.org/biomechanical/article-pdf/doi/10.1115/1.4053143/6806175/bio-21-1259.pdf by Universidad De Zaragoza Biblioteca user on 10 January 2022

Journal of Biomechanical Engineering. Received July 14, 2021;
Accepted manuscript posted December 05, 2021. doi:10.1115/1.4053143
Copyright (c) 2021 by ASME; reuse license CC-BY 4.0

breast cancer, MCF7, which is well known as nonmetastatic, and the MDA-MB-231 cell line, which has a high invasive capability [30].

Methods

1. Design of microfluidic devices for single-cell migration under barotactic stimuli

To better understand how cancer cell migration is affected by confined microenvironments and barotactic stimuli, novel microfluidic devices were fabricated, and tumor cells were left to choose between two paths whose main difference was its hydraulic resistance. These devices were designed with two different heights and have two main functional parts (**Figure 1**): a cell capture site and a decision-making point, as explained later.

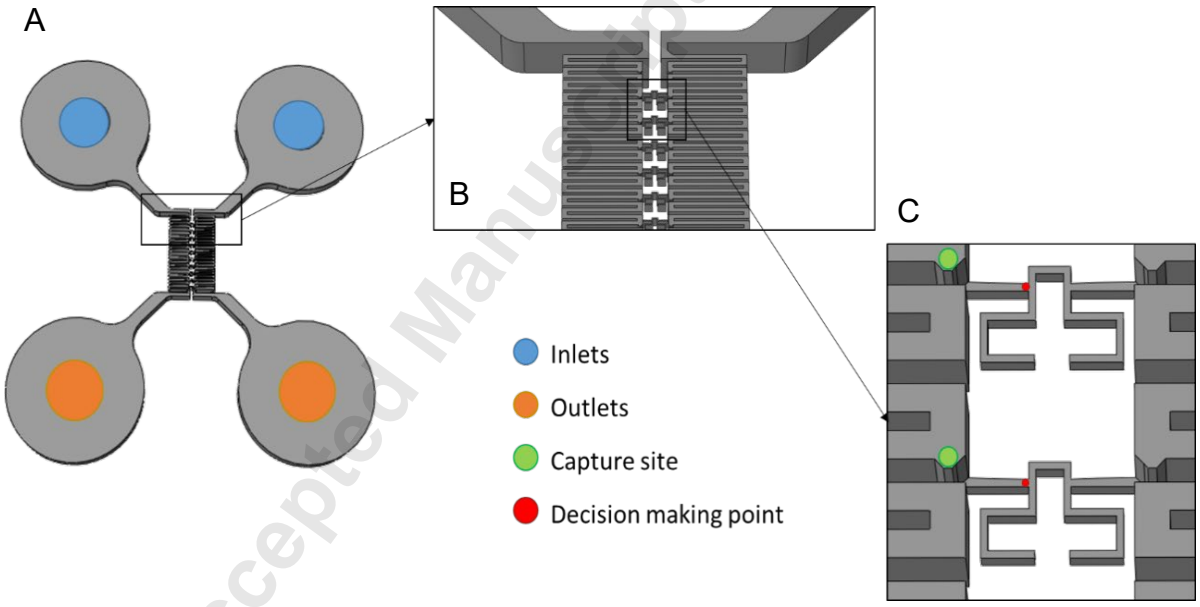

Figure 1: Three-dimensional overview and details of one of the designed devices. (A) Full view in which 40-µm height inlets (blue) and outlets (orange) are connected through the core part of the device. (B) Magnification of the core serpentine paths of 40-µm height and the specific internal geometry of 10-µm height. (C) Details of the 10-µm height capture site (green) and the 10-µm height internal confined geometry (dead-end path in this case). Here, a short and confined channel connects the capture site with the decision-making point (red).

Accepted Manuscript Not Copyedited

Downloaded from http://asmedigitalcollection.asme.org/biomechanical/article-pdf/doi/10.1115/1.4053143/6806175/bio-21-1259.pdf by Universidad De Zaragoza Biblioteca user on 10 January 2022

Journal of Biomechanical Engineering. Received July 14, 2021;
Accepted manuscript posted December 05, 2021. doi:10.1115/1.4053143
Copyright (c) 2021 by ASME; reuse license CC-BY 4.0

The first part of the designed devices consists of a single-cell capture site (**Fig. 1** C) created by a subcellular size hole with lower hydraulic resistance [31]–[36]. These microfluidic chips allow single-cell hydrodynamic capture when cells are loaded through the inlet ports. Capture sites were built with a serpentine path of 40-μm height and 30-μm width and small gaps between its walls (of 10-μm height and 10-μm width) adjacent to the confined channels to improve cell capture and single-cell entry to the confined microchannels. The second part of the designed device consists of a channel (10 μm high and 8 μm wide, with slightly enlarged entrance that was 10 μm high and 10 μm wide) that leads to the decision point, bifurcated into two channels of identical section (10 μm high and 8 μm wide). This channel is located in the middle of the internal geometry, where the cell must migrate through.

Once cells have been trapped at the cell capture site (**Fig. 1** C), they can take several actions: they can either continue through the central channel, migrate through the serpentine, or enter into the confined migration channel in which they will have to choose once in the bifurcation point. At this point, the only difference between the two paths is the hydraulic resistance the cell senses when trying to enter each of the paths [28].

Four internal geometries (**Fig. 2**) were designed: (I) a symmetric device (**Fig. 2** A), used as a negative control, where the decision paths (top path and bottom path) are identical, as well as their hydraulic resistances, and the cells are expected to adopt a random choice; (II) a twisted device (**Fig. 2** B) in which one of its paths is twisted and therefore has a higher length and higher hydraulic resistance (long path and short path); (III) a dead-end device (**Fig. 2** C), exhibiting one path where there is no exit (dead-end path and open path) to maximize the hydraulic-resistance difference between both paths (as the only outflow is occluded by the presence of the cell) [37]; and finally, (IV) a tortuosity device (**Fig. 2** D), where the two decision paths present similar lengths but different levels of tortuosity (high-tortuosity path and low-tortuosity path).

2. Polydimethylsiloxane (PDMS)-based microfluidic devices

PDMS-based microfluidic devices were fabricated as described by Shin *et al.* [38]. Briefly, soft lithography was used to develop two aligned heights of positive SU8 molds

Accepted Manuscript Not Copyedited

Downloaded from http://asmedigitalcollection.asme.org/biomechanical/article-pdf/doi/10.1115/1.4053143/6806175/bio-21-1259.pdf by Universidad De Zaragoza Biblioteca user on 10 January 2022

Journal of Biomechanical Engineering. Received July 14, 2021;
Accepted manuscript posted December 05, 2021. doi:10.1115/1.4053143
Copyright (c) 2021 by ASME; reuse license CC-BY 4.0

onto silicon wafers with the desired geometry (MicroLIQUID). Microdevices were fabricated in polydimethylsiloxane (PDMS Sylargd-184, Dow Corning GmbH) at a 10:1 weight ratio for the base to curing agent. The solution was mixed and poured onto the SU8 master and then degassed to remove air bubbles. PDMS was cured at 80 °C for 24 hours, and then, the replica-molded layer was trimmed, perforated and autoclaved. PDMS microdevices were activated with plasma treatment and bonded to 35-mm glass-bottom petri dishes (Ibidi).

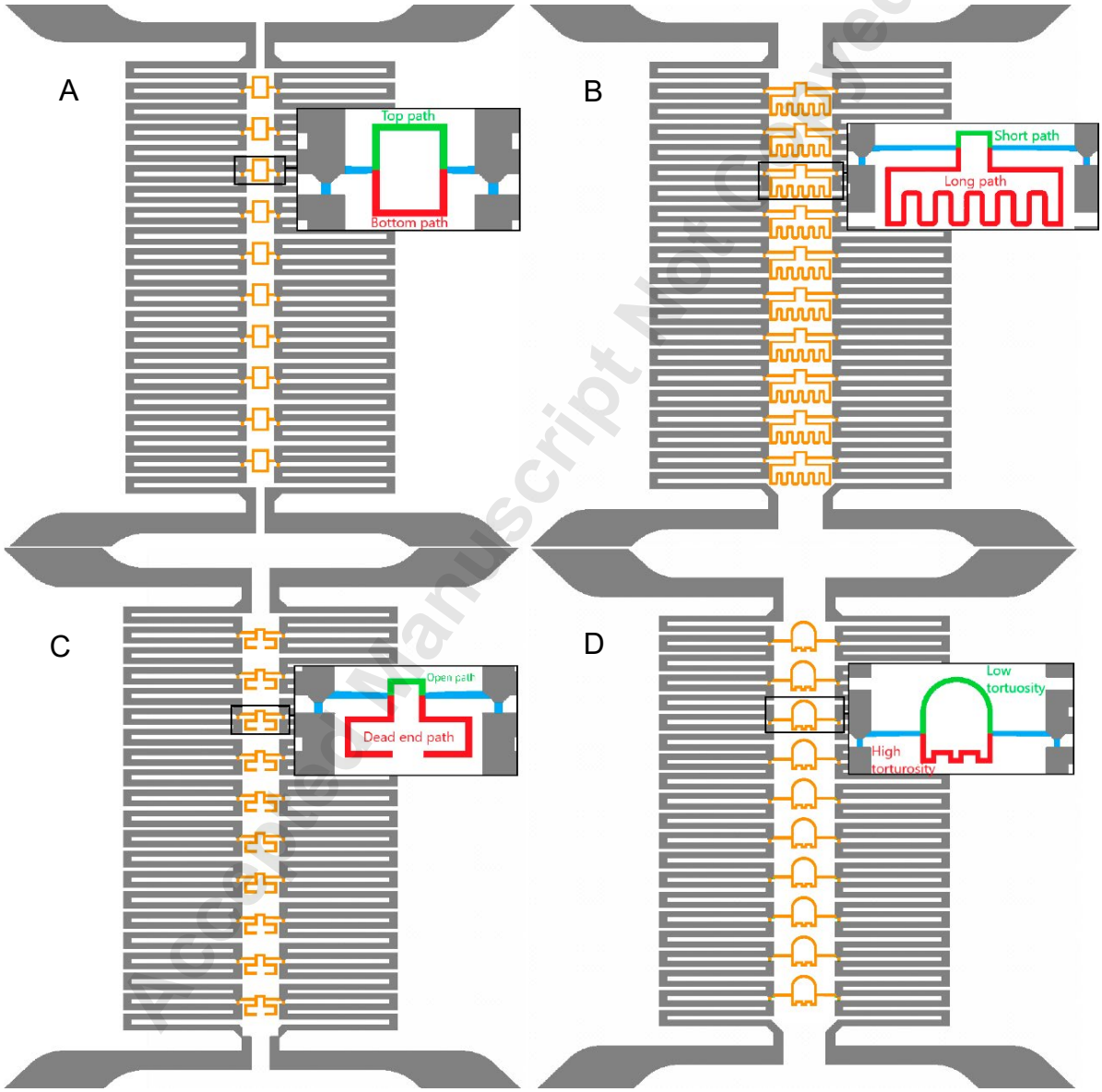

Figure 2: Scheme of the designed devices: gray color identifying 40-µm height structures, and orange color representing 10 µm. Symmetric device (A), Twisted device (B), Dead-end device (C) and Tortuosity device (D). The zoom at the central part of the device shows the possible migration paths for the barotactic study in green and red.

Accepted Manuscript Not Copyedited

Downloaded from http://asmedigitalcollection.asme.org/biomechanical/article-pdf/doi/10.1115/1.4053143/6806175/bio-21-1259.pdf by Universidad De Zaragoza Biblioteca user on 10 January 2022

Journal of Biomechanical Engineering. Received July 14, 2021;
Accepted manuscript posted December 05, 2021. doi:10.1115/1.4053143
Copyright (c) 2021 by ASME; reuse license CC-BY 4.0

Collagen type I (20 μg/mL) was coated for 1 hour at 37 °C to facilitate cell adhesion. After incubation, the microdevices were cleaned with phosphate buffered saline (PBS, Gibco) and Dulbecco's modified Eagle's medium (DMEM, Gibco). Once the device was fully primed with culture media, cells resuspended at a concentration of 1.5 $\times 10^6$ cells/ml of complete media were loaded *via a* static head (70 μl) onto the left inlet with the same volume of complete media in the right inlet (**Fig. 1** A). Cells were allowed to flow by the serpentine path (**Fig. 1** B), and after they were trapped in the capture sites (**Fig. 1** C), the fluid flow was stopped by adding complete media on the outlets. To avoid pressure drops between inlets, outlets and the counterpart serpentine paths that could interfere with the cell performance, microdevices were allowed to settle for 30 min at 37 °C before image acquisition. Therefore, the device reaches static conditions, and the behavior of the cells during the experiment was exclusively based on the features of the channels. Hence, barotaxis can be measured, as the confined migration of the cells requires them to generate pressure to push the fluid ahead. The minimal pressure required for cell migration in one channel is proportional to the hydraulic resistance of that channel (defined by its length and tortuosity, being the cross section constant among all the channels) [24], [26].

3. Image acquisition and analysis

Cell migration was visualized and recorded *via* time-lapse live microscopy (Nikon-Eclipse Ti) at 37 °C in a humidified atmosphere of 5% CO_2. The microscope was equipped with a cell culture chamber, which maintained ideal temperature, humidity and O_2/CO_2 conditions for cell culture. Phase-contrast time-lapse images were taken for 18 h in a 5-min interval and using a 10× objective. Only single and viable captured cells were tracked over time. Manual counting following the acquired images was performed to assess confined channel internalization and to evaluate migration path decisions among those cells that reached the confined bifurcation point. Between 4 and 8 devices of each different geometry were tested per cell line. In addition, migration speed measures to calibrate fluid flow simulations were carried out *via* the ImageJ manual tracking plug-in (National Institutes of Health, USA).

Accepted Manuscript Not Copyedited

Downloaded from http://asmedigitalcollection.asme.org/biomechanical/article-pdf/doi/10.1115/1.4053143/6806175/bio-21-1259.pdf by Universidad De Zaragoza Biblioteca user on 10 January 2022

Journal of Biomechanical Engineering. Received July 14, 2021;
Accepted manuscript posted December 05, 2021. doi:10.1115/1.4053143
Copyright (c) 2021 by ASME; reuse license CC-BY 4.0

4. Quantification of the hydraulic resistance

To understand the barotactic stimulus that cells sense at the decision-making point (**Fig. 1**), we evaluated the hydraulic resistance of the channel by two different methods. On the one hand, we computationally simulated the two-dimensional steady fluid flow to study the difference in the hydraulic resistance between the paths of each microdevice. On the other hand, theoretical approximations of the hydraulic resistance of some straight channels were estimated following previous theoretical works [26]. However, with this theoretical approximation, the hydraulic losses produced in elbow pipping are understimated. In the case of the tortuosity microdevice, since the lengths of the two channels are similar, the losses produced in the change in direction of the pipping could modify the expected hydraulic resistance, affecting barotaxis. A comparison between the two methods is included in Supplementary material 1.

To better understand the hydraulic resistances at the decision-making point, we performed fluid flow simulations of the microdevices by means of the finite volume method (FVM) in Ansys Fluent 2019 R2. The details of the fluid flow simulations have been incorporated in Supplementary material 2. Moreover, to validate the computational fluid flow simulations and to guarantee the independence of the mesh on the solution, we performed a mesh convergence analysis by means of the grid convergence index (GCI) presented by Roache [39] (Supplementary material 3).

5. Cell Lines

Human breast cancer cell lines were chosen since breast cancer is a major malignancy among cancers; it leads the number of cancer-related deaths in women worldwide, and its incidence continues to rise annually [40], [41]. MCF7 and MDA-MB-231 cells were purchased from the European Collection of Authenticated Cell Cultures (ECACC) as models of nonmetastatic and metastatic tumors. The cells were cultured at 37 °C in a humidified atmosphere of 5% CO_2. They were routinely grown in DMEM-high glucose (Gibco) supplemented with 10% heat-inactivated fetal bovine serum (FBS, Gibco) and 1% antibiotic-antimycotic solution of penicillin, streptomycin and amphotericin B (Gibco). Nearly 1000 cells of both types were tested in total, and more than 70 were used for the hydraulic-resistance cell decision. Single cell size was

Accepted Manuscript Not Copyedited

Downloaded from http://asmedigitalcollection.asme.org/biomechanical/article-pdf/doi/10.1115/1.4053143/6806175/bio-21-1259.pdf by Universidad De Zaragoza Biblioteca user on 10 January 2022

Journal of Biomechanical Engineering. Received July 14, 2021;
Accepted manuscript posted December 05, 2021. doi:10.1115/1.4053143
Copyright (c) 2021 by ASME; reuse license CC-BY 4.0

measured in suspended cells immediately after trypsinization using NIS-Element software (Nikon).

6. Cell migration within 3D extracellular matrix

Alternative microdevices [20] were fabricated to host extracellular matrices (ECM), following the methodology in Methods Section 2 and the remaining steps of the Shin et al. protocol for cell culture within hydrogels in microfluidic devices.

Collagen gels of 2.5 mg/ml concentration and pH 7.4 were created by mixing collagen type I (BD Bioscience), NaOH, Dulbecco's phosphate buffered saline, DPBS (Thermo Fisher), and culture medium with suspended cells (after trypsinization and centrifugation). MCF-7 and MDA-MB-231 cells were mixed with gel solutions at a final concentration of 2×10^5 cells/ml and pipetted into the gel cavities of the microdevice, as in previous reports [20], [42]–[46].

Subsequent to filling the gel scaffold regions, the devices were placed in prepared humid chambers within a CO_2 incubator to allow the collagen to polymerize at 37 °C for 20 min. After polymerization, the gels were hydrated with DMEM and left in the incubator for 24 h beforehand to ensure the stabilization of the matrix and cell adhesion and conditioning. Then, MCF-7 or MDA-MB-231 cells within the 3D extracellular matrix were subjected to phase-contrast imaging every 20 min for 24 h *via* time-lapse live microscopy at 37 °C in a humidified atmosphere of 5% CO_2. The focal plane located in the middle of the device along the z-axis was selected, which was more than 100 μm away from the 2D surfaces of the device, ensuring fully embedded cells were analyzed [20], [42]. Cell trajectory acquisition was performed using a hand-coded semiautomatic MATLAB script described in previous studies [20], [42]–[46]. These trajectories were used to extract the mean speed and effective velocity, defined as the average instantaneous speed including all time steps and speed from the initial to the final position, respectively.

Accepted Manuscript Not Copyedited

Downloaded from http://asmedigitalcollection.asme.org/biomechanical/article-pdf/doi/10.1115/1.4053143/6806175/bio-21-1259.pdf by Universidad De Zaragoza Biblioteca user on 10 January 2022

Journal of Biomechanical Engineering. Received July 14, 2021;
Accepted manuscript posted December 05, 2021. doi:10.1115/1.4053143
Copyright (c) 2021 by ASME; reuse license CC-BY 4.0

Results

1. Microfluidic-based chips with different channel configurations allow the achievement of a diverse variety of barotactic stimuli that could be sensed by tumor cells.

To explore how mechanical factors can regulate cancer cell migration under physical confinement, we designed four microfluidic devices: a symmetric device, a twisted device, a dead-end device, and a tortuosity device (**Fig. 2**). The double height design allowed both the capture of individual cells and the connection of the loading cell ports to the confined area, where cells are tested against different hydraulic resistances. These devices enabled the isolation of mechanical factors from chemical factors and allowed the study of barotaxis and hydraulic resistance of individual cancer cells by decision-making.

To control the hydraulic resistance of the different paths, we studied the contours of the velocity magnitude and the velocity profile of the microdevices (**Fig. 3**). The velocity magnitude was higher in the lower hydraulic resistance paths and, as the sections were the same, it was proportional to the flow. Overall, the velocity at the walls was equal to zero to guarantee the no-slip condition at the boundary layers and the maximum at the center point of the section, which results in a classic velocity parabolic profile. In the case of the symmetric device (**Fig. 3** A), since the length and tortuosity of the paths are the same, the velocity profiles in both paths were identical, which means that there was no different hydraulic resistance between them. In the twisted device (**Fig. 3** B), the velocity in the short path was significantly higher than that in the long path. In particular, the flow along the short path was approximately twelve times higher than that along the long path, which represented approximately 92.5% of the inlet flow. In this asymmetric configuration, a hydraulic resistance difference of 85% was achieved. In the case of the dead-end microdevice (**Fig. 3** C), the fluid flowed in the open path since the dead-end path was closed and did not allow any flow, maximizing the hydraulic resistance difference between the channels. Finally, in the tortuosity microdevice (**Fig. 3** D), the velocities in both paths were very similar. The inlet flow was divided into 48.75% toward the low-tortuosity path and 51.25% toward the high-tortuosity path; therefore, the hydraulic resistance of the high-

Accepted Manuscript. Not Copyedited

Downloaded from http://asmedigitalcollection.asme.org/biomechanical/article-pdf/doi/10.1115/1.4053143/6806175/bio-21-1259.pdf by Universidad De Zaragoza Biblioteca user on 10 January 2022

Journal of Biomechanical Engineering. Received July 14, 2021;
Accepted manuscript posted December 05, 2021. doi:10.1115/1.4053143
Copyright (c) 2021 by ASME; reuse license CC-BY 4.0

tortuosity path was 2.5% lower than that of the low-tortuosity path (Supplementary material 1. **Table S1**).

2. MDA-MB-231 metastatic cells tend to migrate through paths of lower hydraulic resistance.

After the computational study of the microfluidic properties of the devices, different human breast adenocarcinoma cells (nonmetastatic MCF7 and metastatic MDA-MB-231) were seeded in the devices. Once the cells were captured by the cell-single traps, the microfluidic chips were equilibrated and allowed to settle before time-lapse imaging.

Our results show that despite the nonmetastatic features of MCF7 cells, they were surprisingly not able to reach decision-making sites (Supplementary Material 4. **Video S1**) in any of the internal geometries. They did not seem to have the ability to migrate in the confined microchannel (10 μm high and 8 μm wide). However, this was not observed for the metastatic MDA-MB-231 cells, which entered and moved along the confined microchannels in an apparently easy manner.

Accepted Manuscript Not Copyedited

Downloaded from http://asmedigitalcollection.asme.org/biomechanical/article-pdf/doi/10.1115/1.4053143/6806175/bio-21-1259.pdf by Universidad De Zaragoza Biblioteca user on 10 January 2022

Journal of Biomechanical Engineering. Received July 14, 2021;
Accepted manuscript posted December 05, 2021. doi:10.1115/1.4053143
Copyright (c) 2021 by ASME; reuse license CC-BY 4.0

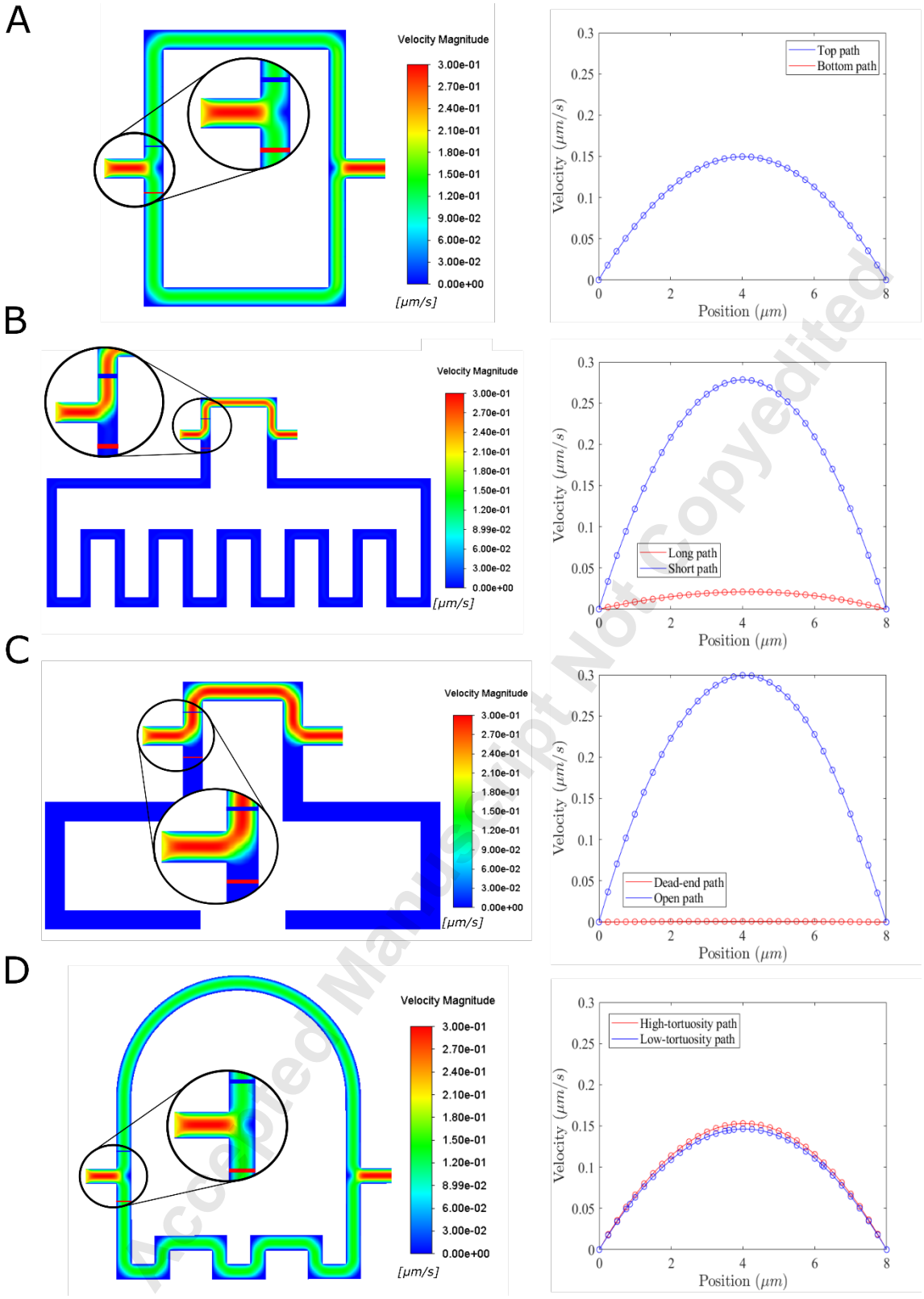

Figure 3: Contours of the velocity magnitude ($\mu m/s$) (left) and the velocity profile (right) among the two paths of the symmetric microdevice (A), the twisted microdevice (B), the dead-end microdevice (C), and the tortuosity microdevice (D). The velocity profiles of each microdevice correspond to the sections marked in blue and red in the magnified detail of the contours.

Accepted Manuscript Not Copyedited

Downloaded from http://asmedigitalcollection.asme.org/biomechanical/article-pdf/doi/10.1115/1.4053143/6806175/bio-21-1259.pdf by Universidad De Zaragoza Biblioteca user on 10 January 2022

Journal of Biomechanical Engineering. Received July 14, 2021;
Accepted manuscript posted December 05, 2021. doi:10.1115/1.4053143
Copyright (c) 2021 by ASME; reuse license CC-BY 4.0

To assess whether hydraulic resistance affects the decision-making of individual cancer cells, the MDA-MB-231 cells were allowed to migrate within the different designed microdevices.

In the symmetric device (**Fig. 4**), which offered the same hydraulic resistance on both paths, MDA-MB-231 cells seemed to show no preference path of migration (45 vs. 55%, devices 7, cells 18), as expected. However, we observed a marked decrease in cell migration toward high hydraulic resistance paths when using asymmetric devices (Twisted device) compared to the path with shorter length and therefore lower resistance (65% of them preferred the lower resistance channel, devices 8, cells 26) (**Fig. 4**).

To investigate the effect of barotaxis in metastatic cells more thoroughly, we developed a design that presented a dead-end path. In this scenario, the path that leads to the dead end would pose higher hydraulic resistance since cells could not push the fluid any further from the wall. The results (**Fig. 4**) revealed that 77% of the cells chose the open path channel to migrate (devices 6, cells 13).

In addition, we sought to understand whether the tortuosity of the paths could also influence the decision-making process. For this reason, new migration channels were designed with similar lengths and hydraulic resistances but different degrees of tortuosity. As shown (**Fig. 4**), MDA-MD-231 cancer cells presented a higher predisposition to migrate through the high-tortuosity path (devices 4, cells 16).

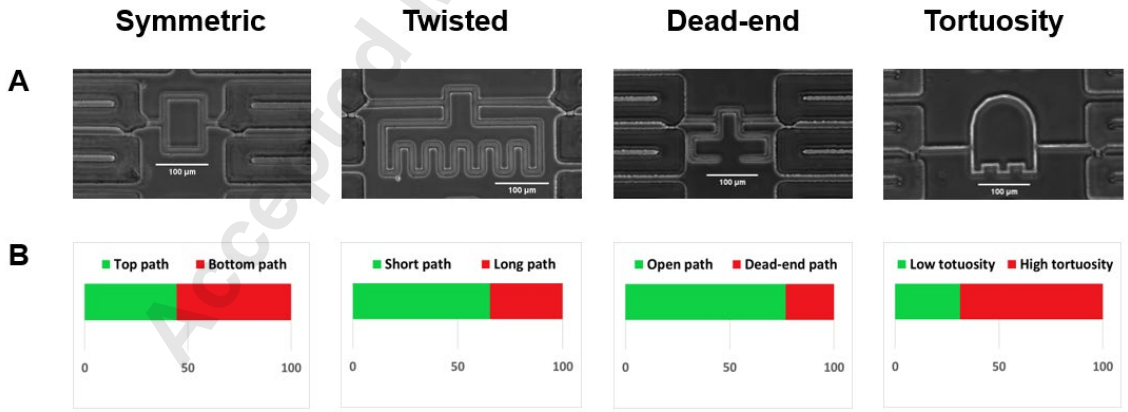

Figure 4: Cell decision per device type. (A) Microscopy image of the internal geometry of each device; the scale bar represents 100 μm. (B) Results from cell decision in confined channels expressed as the percentage of cells that migrate through each possible path. Each color represents a different migration

Accepted Manuscript Not Copyedited

Downloaded from http://asmedigitalcollection.asme.org/biomechanical/article-pdf/doi/10.1115/1.4053143/6806175/bio-21-1259.pdf by Universidad De Zaragoza Biblioteca user on 10 January 2022

Journal of Biomechanical Engineering. Received July 14, 2021;
Accepted manuscript posted December 05, 2021. doi:10.1115/1.4053143
Copyright (c) 2021 by ASME; reuse license CC-BY 4.0

path as previously shown (as a summary, green for upper paths and red for inferior paths). All experiments were conducted in at least four independent assays (n=4), as shown in the text, with total cell counts per type of device being 18, 26, 13 and 16.

A representative video of cell migration for each geometry is shown in Supplementary material 4. **Videos S2, S3, S4, and S5**.

3. MDA-MB-231 metastatic cells migrate faster and more effectively than MCF-7 nonmetastatic cells within a 3D ECM.

To corroborate whether the migration capabilities exhibited within confined microchannels could be extrapolated to extracellular matrices, we studied MCF-7 and MDA-MB-231 cell migration within 3D collagen type I for 24 h. Our results showed that MDA-MB-231 cells were significantly faster than MCF-7 cells (mean speed, **Fig. 5** A) and were much more effective in their migration (effective velocity, **Fig. 5** B).

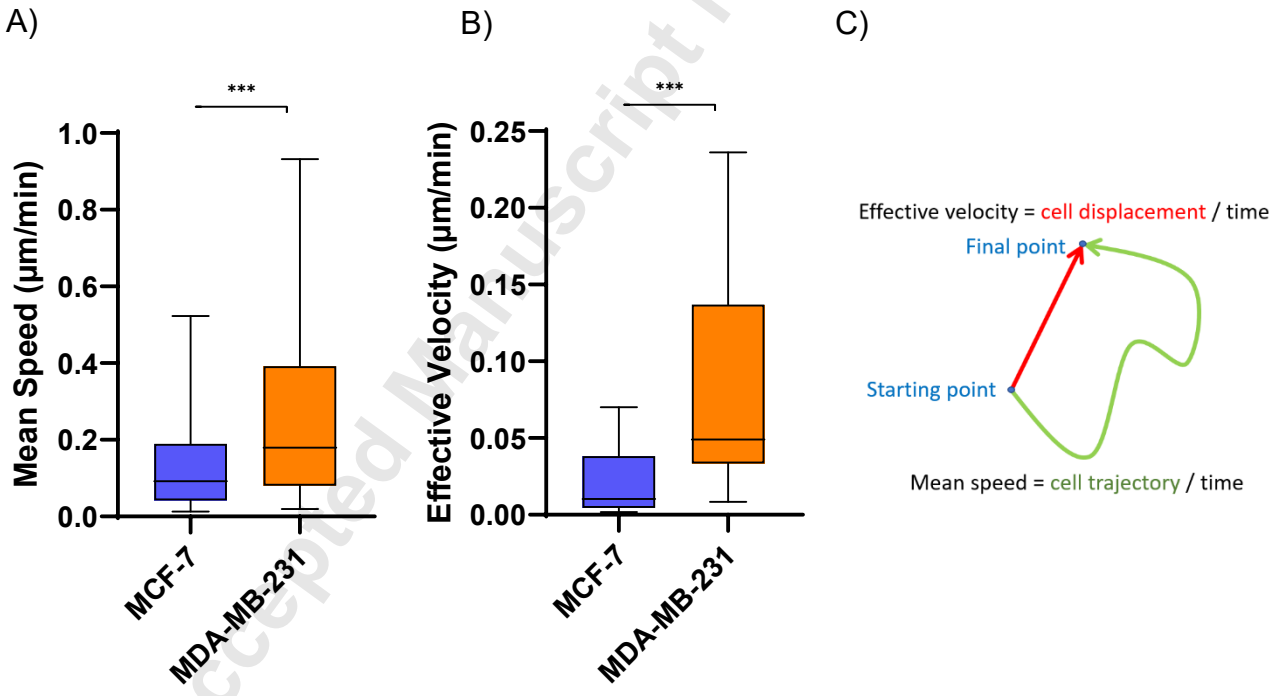

Figure 5: A) Mean speed and B) effective velocity of MCF-7 and MDA-MB-231 cells in 2.5 mg/ml 3D collagen type I gels. C) Outline indicating how the plotted parameters were calculated. Two independent devices per condition (n=2) were used to study more than 90 cells and 6700 data points in total. ANOVA followed by post hoc Tukey–Kramer tests were performed to determine statistical significance: ***p < 0.001.

Accepted Manuscript Not Copyedited

Downloaded from http://asmedigitalcollection.asme.org/biomechanical/article-pdf/doi/10.1115/1.4053143/6806175/bio-21-1259.pdf by Universidad De Zaragoza Biblioteca user on 10 January 2022

Journal of Biomechanical Engineering. Received July 14, 2021;
Accepted manuscript posted December 05, 2021. doi:10.1115/1.4053143
Copyright (c) 2021 by ASME; reuse license CC-BY 4.0

Discussion

Here, we have presented new devices to trap single cancer cells and evaluate their behavior under confined paths and different hydraulic resistances. Our approach relies on recreating diverse restrictive 3D physiological environments, which are crucial aspects of tumor metastasis. Therefore, we have been able to determine the capacity of certain breast tumor cell lines 1) to get inside of, and 2) to migrate through confined spaces, as well as 3) to evaluate their migratory barotaxis-based decisions of metastatic cells. Replicating key steps for tumor cell spreading and metastasis formation will help to evaluate their metastatic potential and in turn increase the number of drug targets as well as the chances of survival of patients.

Our results seem to exhibit a difference in constriction capabilities as well as migration behavior between cells with different metastatic potentials. Whereas 30% of metastatic MDA-MB-231 cells entered the confined channel (10 μm × 10 μm), a key step in the metastasis process [9], only 9% of nonmetastatic MCF7 cells succeeded (nearly 1000 cells tested in total). A similar performance was observed in Yankaskas *et al.* [47], where 100-μm^2 channels (10 μm × 10 μm) allowed the entrance of 3% MCF7 and 20% MDA-MB-231. Furthermore, low metastatic cancer cells (SKOV3) managed it with 5% of the cells in slightly smaller channels (60 μm^2: 10 μm × 6 μm) [31]. In addition, we quantified that while one-third of the MDA-MB-231 cells that entered the confined channel were able to reach the decision point, none of the MCF7 cells achieved it.

The behavior exposed by MCF7 cells, typically characterized as nonmetastatic, paves the way for the implementation of such microdevices to determine the inherent migratory capability and to screen the metastatic potential of certain cancer cells. The results are in agreement with previously published work [48], which showed that under chemotactic stimulus with fetal bovine serum (FBS), MCF7 cells were almost unable to enter and migrate through confined channels even of a 200-μm^2 (10 μm × 20 μm) section. However, FBS chemical stimulus was able to generate migration of MDA-MB-231 through channels that were nearly 10 times smaller [48]. This difference in migration abilities was also found within the 3D extracellular matrix (**Fig. 5**). MDA-MB-231 cells exhibited significantly faster and more directed migration than MCF-7 cells.

Accepted Manuscript Not Copyedited

Downloaded from http://asmedigitalcollection.asme.org/biomechanical/article-pdf/doi/10.1115/1.4053143/6806175/bio-21-1259.pdf by Universidad De Zaragoza Biblioteca user on 10 January 2022

Journal of Biomechanical Engineering. Received July 14, 2021;
Accepted manuscript posted December 05, 2021. doi:10.1115/1.4053143
Copyright (c) 2021 by ASME; reuse license CC-BY 4.0

Therefore, all these data seem to suggest both a reduced ability of MCF-7 cells to enter and migrate within the channels in comparison with MDA-MB-231 cells (as well as within 3D ECM). Furthermore, the previously observed spontaneous movement of confined cells [49] might not affect all cancer cells equally, considering the results found here.

The size of the microfluidic device channels was designed following Irimia recommendations for confined cancer cell migration [50], as well as other previously published works [48], [49], in which a maximum migration speed was reported within channels of 75-μm^2 cross section [49]. The 80-μm^2 section channels (10 μm × 8 μm) ensure that both MCF7 and MDA-MB-231 cell sizes allow them to enter and be confined within these channels. The 19.39-μm (± 2.82 μm SD.) and 16.78 μm (± 2.39 μm) diameters found respectively in MCF7 and MDA-MB-231 cells were similar to those of previous literature results [51], [52]. In addition, given the ability of tumor epithelial cells to migrate in the absence of an extracellular matrix coating [49], we tested (results not shown) whether cells could enter the 80-μm^2 section channels. We found that neither MCF7 nor MDA-MB-231 cells were able to squeeze into the channels. Thus, the channel entrance was slightly enlarged (up to 100 μm^2: 10 μm × 10 μm), creating a funnel-like shape that could facilitate the process. The cross-sectional area of the channel has always been very far from the 7 μm^2 (2.65 μm × 2.65 μm) around which cell arrest is usually produced in tumor cells [53]. Nevertheless, no improvement was shown either with the enlarged section, suggesting that an external protein network is necessary for their entrance and consequent movement. Other strategies, such as culture medium pretreatment (alone) [32] or detergent pretreatment [54], were dismissed because of their inefficacy or interference with cell permeability.

Furthermore, taking advantage of the spontaneous movement of mechanically constrained cells [49], [55], these devices present microchannels with a geometry that forces cells to make a decision on which path to migrate. Their choice is based exclusively on the hydraulic resistance perceived by the individual cells, since they are under confined conditions, mimicking biological pre-existent structures and microchannel structures created by the ECM degradation of metalloproteinases [56]. The importance of such hydraulic resistance in cell mechanics, known as barotaxis, has been previously pointed out, showing that it can regulate polarization and cell

Accepted Manuscript Not Copyedited

Downloaded from http://asmedigitalcollection.asme.org/biomechanical/article-pdf/doi/10.1115/1.4053143/6806175/bio-21-1259.pdf by Universidad De Zaragoza Biblioteca user on 10 January 2022

Journal of Biomechanical Engineering. Received July 14, 2021;
Accepted manuscript posted December 05, 2021. doi:10.1115/1.4053143
Copyright (c) 2021 by ASME; reuse license CC-BY 4.0

motility [27]. However, whether this mechanism may drive metastasis in cancer or not is still an unsolved question.

In our model, metastatic breast cells preferentially migrated through fewer resistance paths. This directional bias becomes more evident as the hydraulic resistance difference increases. Our results agree with Prentice-Mott *et al.* [28], who showed that lymphocytes have an enhanced preference for the less resistant channel to migrate. Nevertheless, unlike lymphocytes, we observed that MDA-MB-231 cells also seem to be able to migrate through the more resistant channels in more than 20% of the cells. These results could be validated by other devices with comparable data [57], [58], which suggested the use of the Osmotic Engine Model (OEM) in MDA-MB-231 cells to migrate through highly resistant channels. This mechanism, based on cell permeability and polarization, is able to generate a water flux through the cell and, in the end, cell displacement [25]. Then, although metastatic cancer cells seem to sense and tend to migrate through the lowest resistant channels, they may have underlying mechanisms, such as OEM or their ability to squeeze [48], that allow them to overcome some difficulties encountered in the migration journey.

Moreover, with the aim of unraveling novel and unknown features influencing cancer cell migration, we built a tortuosity microdevice, whose bottom channel presents a higher level of tortuosity than the top channel, because of the number of bends that the path has compared to the top channel. In this configuration, the high-tortuosity path is slightly shorter than the low-tortuosity path to compensate for the hydraulic losses produced in the changes in the flow direction in elbow piping (Supplementary Material 1). Thus, we achieved a microdevice with two channels with similar hydraulic resistances that permitted us to study whether the topology might affect the cell capacity to sense hydraulic resistances. Despite the fact that a light deviation in the cell migration toward the high-tortuosity path could be expected, the results show a marked preference in migrating through the high-tortuosity path than through the low-tortuosity path. These could be attributed to the slight differences in hydraulic resistance or the differential tortuosity of the channel, suggesting that still unknown mechanisms might play a part in cancer cell migration regarding the large variety of migration modes [9] as well as the still elusive interplay of the biophysical variables, such as confinement, topology, adhesion or rigidity [59].

Accepted Manuscript Not Copyedited

Downloaded from http://asmedigitalcollection.asme.org/biomechanical/article-pdf/doi/10.1115/1.4053143/6806175/bio-21-1259.pdf by Universidad De Zaragoza Biblioteca user on 10 January 2022

Journal of Biomechanical Engineering. Received July 14, 2021;
Accepted manuscript posted December 05, 2021. doi:10.1115/1.4053143
Copyright (c) 2021 by ASME; reuse license CC-BY 4.0

Despite the many attempts to understand cancer metastasis and the increasing use of microfluidics [60]–[62], few devices have been designed and used to elucidate cancer cell migration in confined environments that specifically target barotaxis. Nevertheless, although not based on this type of taxis, they have already been proven to be a potential tool to predict the clinical outcomes and metastatic propensity of diverse tumors [47].

To our knowledge, this work originally presents a microfluidic-based study that integrates cancer cell migration through confined spaces and the analysis of metastasis capability based on a barotactic cell decision. However, future experiments will increase the number of cells and will diversify the metastatic potential of the cells tested to overcome the main limitations of this work.

Funding Data

This work was funded by the Spanish Ministry of Science and Innovation (Grant no: RTI2018-094494-B-C21) co-funded with European Union ERDF funds (European Regional Development Fund). Y.J.-L. acknowledges funding support from the Spanish Ministry of Science and Innovation (FPU17/03867). D.C.-G. and P.E.G. also acknowledge funding from the PRIMAGE (PRedictive In-silico Multiscale Analytics to support cancer personalized diaGnosis and prognosis, empowered by imaging biomarkers), a Horizon 2020|RIA project (Topic SC1-DTH-07-2018), grant agreement no: 826494. P.E.G. acknowledges funding from the RIS3-LMP74-18 CELLBIOPRINT project. In addition, S.H.-R. acknowledges funding support from the Government of Aragon (grant 2019-23). The authors would also like to acknowledge the use of Servicio General de Apoyo a la Investigación-SAI, Universidad de Zaragoza.

References

[1] D. Hanahan and R. A. Weinberg, «Hallmarks of cancer: The next generation», *Cell*, vol. 144, no 5. p. 646-674, 2011.

Accepted Manuscript Not Copyedited

Downloaded from http://asmedigitalcollection.asme.org/biomechanical/article-pdf/doi/10.1115/1.4053143/6806175/bio-21-1259.pdf by Universidad De Zaragoza Biblioteca user on 10 January 2022

Journal of Biomechanical Engineering. Received July 14, 2021;
Accepted manuscript posted December 05, 2021. doi:10.1115/1.4053143
Copyright (c) 2021 by ASME; reuse license CC-BY 4.0

[2] T. N. Seyfried and L. C. Huysentruyt, «On the origin of cancer metastasis», *Crit. Rev. Oncog.*, vol. 18, no 1-2, p. 43-73, 2013.

[3] C. L. Chaffer and R. A. Weinberg, «A perspective on cancer cell metastasis», *Science*, vol. 331, no 6024. p. 1559-1564, 2011.

[4] X. Guan, «Cancer metastases: Challenges and opportunities», *Acta Pharm. Sin. B.*, vol. 5, no 5. p. 402-418, 2015.

[5] J. Yang, P. Antin, G. Berx, C. Blanpain, T. Brabletz, M. Bronner, K. Campbell, A. Cano, J. Casanova, G. Christofori, S. Dedhar, R. Derynck, H. L. Ford, J. Fuxe, A. García de Herreros, G. J. Goodall, A. K. Hadjantonakis, R. Y. J. Huang, C. Kalcheim, R. Kalluri, Y. Kang, Y. Khew-Goodall, H. Levine, J. Liu, G. D. Longmore, S. A. Mani, J. Massagué, R. Mayor, D. McClay, K. E. Mostov, D. F. Newgreen, M. A. Nieto, A. Puisieux, R. Runyan, P. Savagner, B. Stanger, M. P. Stemmler, Y. Takahashi, M. Takeichi, E. Theveneau, J. P. Thiery, E. W. Thompson, R. A. Weinberg, E. D. Williams, J. Xing, B. P. Zhou and G. Sheng, «Guidelines and definitions for research on epithelial–mesenchymal transition», *Nat. Rev. Mol. Cell Biol.*, vol. 21, no 6. p. 341-352, 2020.

[6] J. Massagué and A. C. Obenauf, «Metastatic colonization by circulating tumour cells», *Nature*, vol. 529, no 7586. p. 298-306, 2016.

[7] J. Escribano, M. B. Chen, E. Moeendarbary, X. Cao, V. Shenoy, J. M. Garcia-Aznar ,R. D. Kamm and F. Spill, «Balance of mechanical forces drives endothelial gap formation and may facilitate cancer and immune-cell extravasation», *PLoS Comput. Biol.*, vol. 15, no 5, p. e1006395, 2019.

[8] A. W. Holle, N. G. K. Devi, K. Clar, A. Fan, T. Saif, R. Kemkemer and J. P. Spatz, «Cancer Cells Invade Confined Microchannels via a Self-Directed Mesenchymal-to-Amoeboid Transition», *Nano Lett.*, vol. 19, no 4, p. 2280-2290, 2019.

[9] C. D. Paul, P. Mistriotis and K. Konstantopoulos, «Cancer cell motility: Lessons from migration in confined spaces», *Nat. Rev. Cancer*, vol. 17, no 2, p. 131-140, 2017.

[10] P. Friedl and S. Alexander, «Cancer invasion and the microenvironment: Plasticity and reciprocity», *Cell*, vol. 147, no 5. p. 992-1009, 2011.

[11] S. P. Carey, A. Rahman, C. M Kraning-Rush, B. Romero, S. Somasegar, O. M. Torre, R. M. Williams and C. A. Reinhart-King, «Comparative mechanisms of cancer cell migration through 3D matrix and physiological microtracks», *Am. J. Physiol. - Cell Physiol.*, vol. 308, no 6, p. C436-C447, 2015.

[12] K. Ohashi, S. Fujiwara, and K. Mizuno, «Roles of the cytoskeleton, cell adhesion and rho signalling in mechanosensing and mechanotransduction», *J. Biochem.*, vol. 161, no 3. p. 245-254, 2017.

[13] J. Fares, M. Y. Fares, H. H. Khachfe, H. A. Salhab, and Y. Fares, «Molecular principles of

Accepted Manuscript Not Copyedited

Downloaded from http://asmedigitalcollection.asme.org/biomechanical/article-pdf/doi/10.1115/1.4053143/6806175/bio-21-1259.pdf by Universidad De Zaragoza Biblioteca user on 10 January 2022

Journal of Biomechanical Engineering. Received July 14, 2021;
Accepted manuscript posted December 05, 2021. doi:10.1115/1.4053143
Copyright (c) 2021 by ASME; reuse license CC-BY 4.0

metastasis: a hallmark of cancer revisited», *Signal Transduct. Target. Ther.*, vol. 5, no 1. p. 28, 2020.

[14] A. J. Ridley, M. A. Schwartz, K. Burridge, R. A. Firtel, M. H. Ginsberg, G. Borisy, J. T. Parsons and A. R. Horwitz, «Cell Migration: Integrating Signals from Front to Back», *Science*, vol. 302, no 5651, p. 1704-1709, 2003.

[15] F. Merino-Casallo, M. J. Gomez-Benito, Y. Juste-Lanas, R. Martinez-Cantin, and J. M. Garcia-Aznar, «Integration of in vitro and in silico models using Bayesian optimization with an application to stochastic modeling of mesenchymal 3D cell migration», *Front. Physiol.*, vol. 9, p. 1246, 2018.

[16] M. E. Katt, A. L. Placone, A. D. Wong, Z. S. Xu, and P. C. Searson, «In vitro tumor models: Advantages, disadvantages, variables, and selecting the right platform», *Front. bioeng. biotechnol.*, vol. 4, 2016.

[17] J. Hoarau-Véchot, A. Rafii, C. Touboul, and J. Pasquier, «Halfway between 2D and animal models: Are 3D cultures the ideal tool to study cancer-microenvironment interactions?», *Int. J. Mol. Sci.* vol. 19, no 1. p. 181, 2018.

[18] M. E. Fallon, R. Mathews, and M. T. Hinds, «In Vitro Flow Chamber Design for the Study of Endothelial Cell (patho)physiology», *J. Biomech. Eng.* vol. 144, no 2, p. 020801, 2021.

[19] M. Mak, F. Spill, R. D. Kamm, and M. H. Zaman, «Single-Cell Migration in Complex Microenvironments: Mechanics and Signaling Dynamics», *J. Biomech. Eng.*, vol. 138, no 2, 2016.

[20] J. Plou, Y. Juste-Lanas, V. Olivares, C. del Amo, C. Borau, and J. M. García-Aznar, «From individual to collective 3D cancer dissemination: roles of collagen concentration and TGF-β», *Sci. Rep.*, vol. 8, no 1, 2018.

[21] J. S. Jeon, S. Bersini, M. Gilardi, G. Dubini, J. L. Charest, M. Moretti and R. D. Kamm, «Human 3D vascularized organotypic microfluidic assays to study breast cancer cell extravasation», *Proc. Natl. Acad. Sci. U. S. A.*, vol. 112, no 1, p. 214-219, 2015.

[22] S. W. L. Lee, G. Adriani, R. D. Kamm, and M. R. Gillrie, «Models for Monocytic Cells in the Tumor Microenvironment», *Adv. Exp. Med. Biol*, vol. 1224, p. 87-115, 2020.

[23] A. Gandalovičová, D. Rosel, M. Fernandes, P. Veselý, P. Heneberg, V. Čermák, L. Petruželka, S. Kumar, V. Sanz-Moreno and J. Brábek, «Migrastatics—Anti-metastatic and Anti-invasion Drugs: Promises and Challenges», *Trends Cancer*, vol. 3, no 6, p. 391-406, 2017.

[24] A.-M. Lennon-Duménil and H. D. Moreau, «Barotaxis: How cells live and move under pressure», *Curr. Opin. Cell Biol.*, vol. 72, p. 131-136, 2021.

[25] K. M. Stroka, H. Jiang, S. H. Chen, Z. Tong, D. Wirtz, S. X. Sun and K. Konstantopoulos, «Water permeation drives tumor cell migration in confined microenvironments», *Cell*, vol. 157, no 3, p.

Accepted Manuscript Not Copyedited

Downloaded from http://asmedigitalcollection.asme.org/biomechanical/article-pdf/doi/10.1115/1.4053143/6806175/bio-21-1259.pdf by Universidad De Zaragoza Biblioteca user on 10 January 2022

Journal of Biomechanical Engineering. Received July 14, 2021;
Accepted manuscript posted December 05, 2021. doi:10.1115/1.4053143
Copyright (c) 2021 by ASME; reuse license CC-BY 4.0

611-623, 2014.

[26] H. Bruus, «Theoretical microfluidics», *Oxford Oxford Univ. Press.*, 2011.

[27] Y. Li, K. Konstantopoulos, R. Zhao, Y. Mori, and S. X. Sun, «The importance of water and hydraulic pressure in cell dynamics», *J. Cell Sci.*, vol. 133, no 20, p. jcs240341, 2020.

[28] H. V. Prentice-Mott, C. H. Chang, L. Mahadevan, T. J. Mitchison, D. Irimia, and J. V. Shah, «Biased migration of confined neutrophil-like cells in asymmetric hydraulic environments», *Proc. Natl. Acad. Sci. U. S. A.*, vol. 110, no 52, p. 21006-21011, 2013.

[29] Y. Belotti, D. McGloin, and C. J. Weijer, «Analysis of barotactic and chemotactic guidance cues on directional decision-making of Dictyostelium discoideum cells in confined environments», *Proc. Natl. Acad. Sci.*, vol. 117, no 41, p. 25553-25559, 2020.

[30] S. Gayan, A. Teli, and T. Dey, «Inherent aggressive character of invasive and non-invasive cells dictates the in vitro migration pattern of multicellular spheroid», *Sci. Rep.*, vol. 7, no 1, 2017.

[31] Y. C. Chen, S. G. Allen, P. N. Ingram, R. Buckanovich, S. D. Merajver, and E. Yoon, «Single-cell migration chip for chemotaxis-based microfluidic selection of heterogeneous cell populations», *Sci. Rep.*, vol. 5, no November 2014, p. 9980, 2015.

[32] J. P. Frimat, M. Becker, Y. Y. Chiang, U. Marggraf, D. Janasek, J. G. Hengstler, J. Franzkea and J. West, «A microfluidic array with cellular valving for single cell co-culture», *Lab Chip*, vol. 11, no 2, p. 231-237, 2011.

[33] A. A. Khalili, M. R. Ahmad, M. Takeuchi, M. Nakajima, Y. Hasegawa, and R. M. Zulkifli, «A microfluidic device for hydrodynamic trapping and manipulation platform of a single Biological cell», *Appl. Sci.*, vol. 6, no 2, p. 1-17, 2016.

[34] F. Yesilkoy, R. Ueno, B. X. E. Desbiolles, M. Grisi, Y. Sakai, B. J. Kim and J. Brugger, «Highly efficient and gentle trapping of single cells in large microfluidic arrays for time-lapse experiments», *Biomicrofluidics*, vol. 10, no 1, 2016.

[35] A. A. Khalili and M. R. Ahmad, «Numerical analysis of hydrodynamic flow in microfluidic biochip for single-cell trapping application», *Int. J. Mol. Sci.*, vol. 16, no 11, p. 26770-26785, 2015.

[36] S. Kobel, A. Valero, J. Latt, P. Renaud, and M. Lutolf, «Optimization of microfluidic single cell trapping for long-term on-chip culture», *Lab Chip*, vol. 10, no 7, p. 857-863, 2010.

[37] H. D. Moreau, C. Blanch-Mercader, R. Attia, M. Maurin, Z. Alraies, D. Sanséau, O. Malbec, M. G. Delgado, P. Bousso, J. F. Joanny, R. Voituriez, M. Piel, A. M. Lennon-Duménil, «Macropinocytosis Overcomes Directional Bias in Dendritic Cells Due to Hydraulic Resistance and Facilitates Space Exploration», *Dev. Cell*, vol. 49, no 2, p. 171-188.e5, 2019.

[38] Y. Shin, S. Han, J. S. Jeon, K. Yamamoto, I. K. Zervantonakis, R. Sudo, R. D. Kamm and S. Chung, «Microfluidic assay for simultaneous culture of multiple cell types on surfaces or within

Accepted Manuscript Not Copyedited

Downloaded from http://asmedigitalcollection.asme.org/biomechanical/article-pdf/doi/10.1115/1.4053143/6806175/bio-21-1259.pdf by Universidad De Zaragoza Biblioteca user on 10 January 2022

Journal of Biomechanical Engineering. Received July 14, 2021;
Accepted manuscript posted December 05, 2021. doi:10.1115/1.4053143
Copyright (c) 2021 by ASME; reuse license CC-BY 4.0

hydrogels», *Nat. Protoc.*, vol. 7, no 7, p. 1247-1259, 2012.

[39] P. J. Roache, «Perspective: A method for uniform reporting of grid refinement studies», *J. Fluids Eng. Trans. ASME*, vol. 116, no 3, p. 405-413, 1994.

[40] R. L. Siegel, K. D. Miller, and A. Jemal, «Cancer statistics, 2020», *CA. Cancer J. Clin.*, vol. 70, no 1, p. 7-30, 2020.

[41] F. Bray, J. Ferlay, M. Laversanne, D. H. Brewster, C. G. Mbalawa, B. Kohler, M. Piñeros, E. Steliarova-Foucher, R. Swaminathan, S. Antoni, I. Soerjomataram and D. Forman, «Cancer Incidence in Five Continents: Inclusion criteria, highlights from Volume X and the global status of cancer registration», *Int. J. Cancer*, vol. 137, no 9, p. 2060-2071, 2015.

[42] N. Movilla, C. Borau, C. Valero, and J. M. García-Aznar, «Degradation of extracellular matrix regulates osteoblast migration: A microfluidic-based study», *Bone*, vol. 107, p. 10-17, 2018.

[43] O. Moreno-Arotzena, G. Mendoza, M. Cóndor, T. Rüberg, and J. M. García-Aznar, «Inducing chemotactic and haptotactic cues in microfluidic devices for three-dimensional *in vitro* assays», *Biomicrofluidics*, vol. 8, no 6, p. 064122, 2014.

[44] O. Moreno-Arotzena, C. Borau, N. Movilla, M. Vicente-Manzanares, and J. M. García-Aznar, «Fibroblast Migration in 3D is Controlled by Haptotaxis in a Non-muscle Myosin II-Dependent Manner», *Ann. Biomed. Eng.*, vol. 43, no 12, p. 3025-3039, 2015.

[45] C. Del Amo, V. Olivares, M. Cóndor, A. Blanco, J. Santolaria, J. Asín, C. Borau, J. M. García-Aznar, «Matrix architecture plays a pivotal role in 3D osteoblast migration: The effect of interstitial fluid flow», *J. Mech. Behav. Biomed. Mater.*, vol. 83, p. 52-62, 2018.

[46] S. Pérez-Rodríguez, E. Tomás-González, and J. M. García-Aznar, «3D cell migration studies for chemotaxis on microfluidic-based chips: A comparison between cardiac and dermal fibroblasts», *Bioengineering*, vol. 5, no 2, p.45, 2018.

[47] C. L. Yankaskas, K. N. Thompson, C. D. Paul, M. I. Vitolo, P. Mistriotis, A. Mahendra, V. K. Bajpai, D. J. Shea, K. M. Manto, A. C. Chai, N. Varadarajan, A. Kontrogianni-Konstantopoulos, S. S. Martin, K. Konstantopoulos, «A microfluidic assay for the quantification of the metastatic propensity of breast cancer specimens», *Nat. Biomed. Eng.*, vol. 3, no 6, p. 452-465, 2019.

[48] Z. Q. Tong, E. M. Balzer, M. R. Dallas, W. C. Hung, K. J. Stebe, and K. Konstantopoulos, «Chemotaxis of cell populations through confined spaces at Single-Cell resolution», *PLoS One*, vol. 7, no 1, p. e29211, 2012.

[49] D. Irimia and M. Toner, «Spontaneous migration of cancer cells under conditions of mechanical confinement», *Integr. Biol.*, vol. 1, no 8-9, p. 506-512, 2009.

[50] D. Irimia, «Cell migration in confined environments», *Methods Cell Biol*, vol. 121, p. 141-153, 2014.

Accepted Manuscript Not Copyedited

Downloaded from http://asmedigitalcollection.asme.org/biomechanical/article-pdf/doi/10.1115/1.4053143/6806175/bio-21-1259.pdf by Universidad De Zaragoza Biblioteca user on 10 January 2022

Journal of Biomechanical Engineering. Received July 14, 2021;
Accepted manuscript posted December 05, 2021. doi:10.1115/1.4053143
Copyright (c) 2021 by ASME; reuse license CC-BY 4.0

[51] D. L. Adams, P. Zhu, O. V. Makarova, S. S. Martin, M. Charpentier, S. Chumsri, S. Li, P. Amstutz and C. M. Tang, «The systematic study of circulating tumor cell isolation using lithographic microfilters», *RSC Adv.*, vol. 9, p. 4334-4342, 2014.

[52] S. Connolly, K. McGourty, and D. Newport, «The in vitro inertial positions and viability of cells in suspension under different in vivo flow conditions», *Sci. Rep.*, vol. 10, no 1, 2020.

[53] K. Wolf, M. T. Lindert, M. Krause, S. Alexander, J. T. Riet, A. L. Willis, R. M. Hoffman, C. G. Figdor, S. J. Weiss, P. Friedl, «Physical limits of cell migration: Control by ECM space and nuclear deformation and tuning by proteolysis and traction force», *J. Cell Biol.*, vol. 201, no 7, p. 1069-1084, 2013.

[54] M. H. Wu, «Simple poly(dimethylsiloxane) surface modification to control cell adhesion», *Surf. Interface Anal.*, vol. 41, no 1, p. 11-16, 2009.

[55] S. Hervas-Raluy, J. M. Garcia-Aznar, and M. J. Gomez-Benito, «Modelling actin polymerization: the effect on confined cell migration», *Biomech. Model. Mechanobiol.*, vol. 18, no 4, p. 1177-1187, 2019.

[56] M. Paolillo and S. Schinelli, «Extracellular matrix alterations in metastatic processes», *Int. J. Mol. Sci.*, vol. 20, no 19. p. 4947, 2019.

[57] B. S. Wong, P. Mistriotis, and K. Konstantopoulos, «Exposing cell-itary confinement: Understanding the mechanisms of confined single cell migration», *Adv. Exp. Med. Biol.*, vol. 1092, 2018, p. 139-157.

[58] R. Zhao, A. Afthinos, T. Zhu, P. Mistriotis, Y. Li, S. A. Serra, Y. Zhang, C. L. Yankaskas, S. He, M. A. Valverde, S. X. Sun, K. Konstantopoulos, «Cell sensing and decision-making in confinement: The role of TRPM7 in a tug of war between hydraulic pressure and cross-sectional area», *Sci. Adv.*, vol. 5, no 7, 2019.

[59] G. Charras and E. Sahai, «Physical influences of the extracellular environment on cell migration», *Nat. Rev. Mol. Cell Biol.*, vol. 15, no 12, p. 813-824, 2014.

[60] J. Ruppen, L. Cortes-Dericks, E. Marconi, G. Karoubi, R. A. Schmid, R. Peng, T. M. Marti and O. T. Guenat, «A microfluidic platform for chemoresistive testing of multicellular pleural cancer spheroids», *Lab Chip*, vol. 14, no 6, p. 1198-1205, 2014.

[61] A. Pathak and S. Kumar, «Independent regulation of tumor cell migration by matrix stiffness and confinement», *Proc. Natl. Acad. Sci. U. S. A.*, vol. 109, no 26, p. 10334-10339, 2012.

[62] D. L. Bodor, W. Pönisch, R. G. Endres, and E. K. Paluch, «Of Cell Shapes and Motion: The Physical Basis of Animal Cell Migration», *Dev. Cell*, vol. 52, no 5, p. 550-562, 2020.

Accepted Manuscript Not Copyedited

Downloaded from http://asmedigitalcollection.asme.org/biomechanical/article-pdf/doi/10.1115/1.4053143/6806175/bio-21-1259.pdf by Universidad De Zaragoza Biblioteca user on 10 January 2022

Journal of Biomechanical Engineering. Received July 14, 2021;
Accepted manuscript posted December 05, 2021. doi:10.1115/1.4053143
Copyright (c) 2021 by ASME; reuse license CC-BY 4.0

Supplementary material

1. Hydraulic resistances

In this section, we present a discussion about the hydraulic resistance of the microdevices and a comparison between theoretical and simulated flow rates. Since the sections of the two channels in each microdevice are the same, the hydraulic resistance is dominated by the length of the channel (Bruus, 2011); the higher the length is, the higher the hydraulic resistance it has. Thus, study of hydraulic resistance simplifies the analysis of the length of the paths. The decision-making process of directional cell migration is affected by the relative difference in hydraulic resistance between the two paths. Therefore, an analysis of the flow rates clarifies the hydraulic resistance difference between the channels, as the flow rate will be higher in paths with lower hydraulic resistance. The theoretical flow rates can be obtained by comparing the length of the path with the total length of both paths:

$$Q_{top}(\%) = \left(100 - \frac{L_{top}}{L_{top} + L_{bot}} \cdot 100\right),$$

where L_{top} and L_{bot} are the lengths of the top and bottom paths, respectively. The analysis of the length of the channels and the theoretical and simulated flow rates are presented in **Table S1**. In the case of the symmetric microdevice, the lengths are identical; therefore, there is no difference in the hydraulic resistance between them. In the twisted microdevice, there is a significant difference in the lengths of the long path compared to the short path. In particular, the flow divides approximately 91.84% in the short path and 8.16% in the long path since the difference in the hydraulic resistance of the long path is approximately 83.68% higher concerning the long path. In the case of the dead-end microdevice, the dead-end path is closed and does not allow any flow; therefore, the hydraulic resistance difference is maximized in this configuration. Finally, in the tortuosity microdevice, the high-tortuosity path is slightly shorter than the low-tortuosity path, so it offers a lower hydraulic resistance. However, the theoretical approximation does not take into account the hydraulic losses due to the changes in flow direction in elbow pipping. For this reason, the simulated flow rate updates the flow rates and reduces the flow rate in the high-tortuosity path. Despite this correction, the hydraulic resistance of the high-tortuosity path is lower than that of the low-tortuosity path. Nonetheless, because the flow rates are very similar, the difference in

Accepted Manuscript Not Copyedited

Downloaded from http://asmedigitalcollection.asme.org/biomechanical/article-pdf/doi/10.1115/1.4053143/6806175/bio-21-1259.pdf by Universidad De Zaragoza Biblioteca user on 10 January 2022

Journal of Biomechanical Engineering. Received July 14, 2021;
Accepted manuscript posted December 05, 2021. doi:10.1115/1.4053143
Copyright (c) 2021 by ASME; reuse license CC-BY 4.0

the hydraulic resistance is low, and this configuration permits studying whether the topology might affect the cell capacity to sense hydraulic resistances.

Table S1. Lengths of the microdevice channels and theoretical and simulated flow rates

Microdevices	*Channels*	*Length (µm)*	*Theoretical flow rate*	*Simulated flow rate*
Symmetric	*Bottom path*	173	50%	50%
	Top path	173	50%	50%
Twisted	*Long path*	1159	8.16%	7.50%
	Short path	103	91.84%	92.50%
Dead-end	*Dead-end path*	188	0%	0%
	Open path	75	100%	100%
Tortuosity	*High-tortuosity path*	222	52.16%	51.25%
	Low-tortuosity path	242	47.84%	48.75%

2. Fluid flow simulation

To better understand the hydraulic resistances at the decision-making point, we performed fluid flow simulations of the microdevices by means of the finite volume method (FVM) in Ansys Fluent 2019 R2. The FVM is based on an integral form of the partial differential equations to be solved with the values of the conserved variables averaged across the volume (Jeong and Seong, 2014). It requires the discretization of the domain into finite volumes (or cells), and then for every volume, the governing equations are solved (Ferziger and Perić, 2002). Thus, the microdevice geometries were discretized to create a computational mesh. The meshes were built with quadrilateral elements and with a mapped mesh method to improve the element quality. The chosen element size of the mesh generated for the microdevices was 0.25 µm, and the mean values of the average skewness and orthogonal factor of the microdevices were approximately 0.0154 and 0.9967, respectively (for further details on the mesh convergence analysis, see Supplementary material 3). To solve the flow in the microdevices, we used the material properties of water liquid with a density of 998.2 kg/m^3 and dynamic viscosity of $1.003 \cdot 10^{-3}$ Pa s. The inlet boundary condition was set as a uniform velocity profile with a magnitude of 0.2 µm/s to obtain the magnitude order of the cell migration velocity measured in the channels (results not shown). Therefore, we assumed a laminar flow with a low Reynolds number since the velocity magnitude and characteristic lengths of the microdevices are low. The outlet

Accepted Manuscript Not Copyedited

Downloaded from http://asmedigitalcollection.asme.org/biomechanical/article-pdf/doi/10.1115/1.4053143/6806175/bio-21-1259.pdf by Universidad De Zaragoza Biblioteca user on 10 January 2022

Journal of Biomechanical Engineering. Received July 14, 2021;
Accepted manuscript posted December 05, 2021. doi:10.1115/1.4053143
Copyright (c) 2021 by ASME; reuse license CC-BY 4.0

boundary condition was specified as an atmospheric pressure outlet. The solution methods used were a pressure-velocity coupled scheme with a third-order MUSCL scheme for momentum and a second-order scheme for pressure.

3. Mesh convergence study

To validate the computational fluid flow simulations and to guarantee the independence of the mesh on the solution, we perform a mesh convergence analysis by means of the grid convergence index (GCI) presented by Roache (Roache, 1994). This method, widely used in computational fluid dynamics (CFD) simulations, is based on Richardson's extrapolation and gives an estimation of the uncertainty of the accuracy of the results. For this purpose, three meshes are required to be created and then the convergence parameter is calculated in each mesh to analyze the differences between them. We chose a refinement factor of 2 for grid size reduction, which is the level of refinement mostly used in the literature. From fine to coarse, the element sizes of the meshes were 0.25 μm, 0.5 μm, and 1 μm (namely, *j=1, 2, and 3,* respectively). Moreover, it requires a safety factor for the error calculation, which is recommended to be within the range of 1.25 and 3. We considered a safety factor of 3, which is very conservative for the actual errors.

In this work, we focused on determining the velocity in the microdevice channels. Thus, we obtained the velocity profile in the top path of the microdevices in the three proposed meshes (**Fig. S1**). The velocity profile in the bottom path does not need to be represented because if the top velocity profile converges, then the bottom path does also converge since the mass is conserved. To perform the GCI analysis, we evaluated the convergence of the area under these curves, which were calculated through trapezoidal numerical integration. The results of the GCI are shown in **Table S2**. The parameter $GCI_{j+1,j}$ represents the uncertainty of the magnitude for the fine (j=1) and medium (j=2) meshes. The coarse (j=3) mesh was not computed since there was not a coarser mesh to compare the convergence with. The GCI values for the fine mesh were between 0.87 and 1.63%; therefore, the performance of this mesh is very adequate.

Accepted Manuscript Not Copyedited

Downloaded from http://asmedigitalcollection.asme.org/biomechanical/article-pdf/doi/10.1115/1.4053143/6806175/bio-21-1259.pdf by Universidad De Zaragoza Biblioteca user on 10 January 2022

Journal of Biomechanical Engineering. Received July 14, 2021;
Accepted manuscript posted December 05, 2021. doi:10.1115/1.4053143
Copyright (c) 2021 by ASME; reuse license CC-BY 4.0

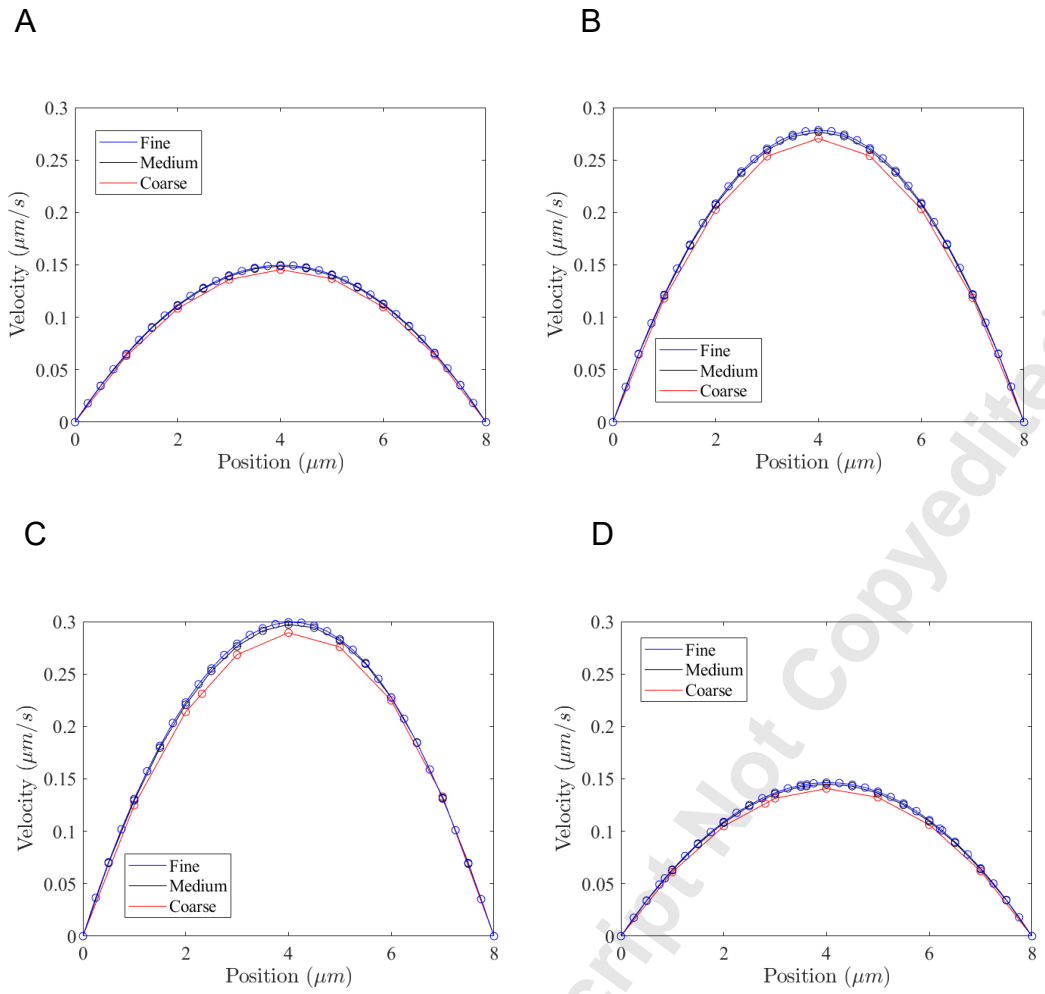

Figure S1. Velocity profiles in the fine, medium and coarse meshes in the top path of the symmetric microdevice in (A), the twisted microdevice in (B), the dead-end microdevice in (C) and the tortuosity microdevice in (D)

Table S2. Mesh convergences of the microdevices

	Symmetric	*Twisted*	*Dead-end*	*Tortuosity*
Grid j	$GCI_{j+1,j}$ (%)	$GCI_{j+1,j}$ (%)	$GCI_{j+1,j}$ (%)	$GCI_{j+1,j}$ (%)
1	0.91	0.89	0.87	1.63
2	3.56	3.51	3.44	5.42

4. Cell migration in confined channels

Video S1. MCF7 cell facing the entrance to the confined channel

Video S2. MDA-MB-231 cell in the Symmetric device

Accepted Manuscript Not Copyedited

Downloaded from http://asmedigitalcollection.asme.org/biomechanical/article-pdf/doi/10.1115/1.4053143/6806175/bio-21-1259.pdf by Universidad De Zaragoza Biblioteca user on 10 January 2022

Journal of Biomechanical Engineering. Received July 14, 2021;
Accepted manuscript posted December 05, 2021. doi:10.1115/1.4053143
Copyright (c) 2021 by ASME; reuse license CC-BY 4.0

Video S3. MDA-MB-231 cell in the Twisted device

Video S4. MDA-MB-231 cell in the Dead-end device

Video S5. MDA-MB-231 cell in the Tortuosity device

5. References of supplementary material

H. Bruus, «Theoretical microfluidics», *Oxford Univ. Press.*, *Oxford,* 2011.

W. Jeong and J. Seong, «Comparison of effects on technical variances of computational fluid dynamics (CFD) software based on finite element and finite volume methods», *Int. J. Mech. Sci.*, vol. 78, p. 19-26, 2014.

J. H. Ferziger and M. Perić, «Computational Methods for Fluid Dynamics», *Springer, Berlin, Heidelberg*, 2002.

P. J. Roache, «Perspective: A method for uniform reporting of grid refinement studies», *J. Fluids Eng. Trans. ASME*, vol. 116, no 3, p. 405-413, 1994.

Accepted Manuscript Not Copyedited

Downloaded from http://asmedigitalcollection.asme.org/biomechanical/article-pdf/doi/10.1115/1.4053143/6806175/bio-21-1259.pdf by Universidad De Zaragoza Biblioteca user on 10 January 2022